Hybrid Control of Fixed-Wing UAVs for Large-Angle Attitude Maneuvers on the Two-Sphere ⋆

Dirk Reinhardt * **Erlend. M. Coates** * **Tor Arne Johansen** *

* *Center for Autonomous Marine Operations and Systems, Norwegian University of Science and Technology, Department of Engineering Cybernetics, Trondheim, 7491 Norway (e-mail: {dirk.p.reinhardt, erlend.m.l.coates, tor.arne.johansen}@ntnu.no).*

Abstract: We propose the design of a hybrid controller for fixed-wing unmanned aerial vehicles which guarantees global exponential tracking of attitude references on the two-sphere. The chosen attitude representation is singularity-free and can be exploited to apply proportional feedback along the shortest path in the natural configuration space, giving it an advantage to conventional design methods based on Euler angle reprentations. The design includes the concept of synergistic potential functions to overcome the problem of a vanishing potential at the additional undesired equilibrium on the compact manifold. It employs proportional-derivative feedback with the relative velocity as an exogeneous input and allows for integration into conventional autopilot architectures. The controller is well-suited for the recovery from large attitude disturbances and the performance is demonstrated in a numerical example.

Keywords: Aircraft control; Autonomous Vehicles; Attitude Control; Hybrid Control

1. INTRODUCTION

In this paper, we present a controller design for exponential tracking of roll/pitch references on the two-sphere, given to a fixed-wing Unmanned Aerial Vehicle (UAV) in order to follow desired climb and turn rates. This is a core function that any autopilot relies on to achieve higher-level control objectives such as path-following. A common control approach is based on Euler angles as a minimal attitude representation that is subject to a singularity referred to as gimbal-lock (Beard and McLain, 2012). This is not an issue in normal flight conditions, but may cause problems in situations where the aircraft is in agile flight or has to recover from severe wind disturbances (Johansen et al., 2014). One possible remedy is to design the controller directly on the configuration manifold where the corresponding attitude is unique and globally defined. The attitude of the aircraft is represented by elements of SO(3), which is the set of 3-by-3 rotation matrices. Stabilizing attitude references on this manifold would constrain the yaw angle and therefore not result in a well-defined control problem in a bank-to-turn maneuver where the yaw motion is typically controlled indirectyly through the roll angle (Beard and McLain, 2012). Possible approaches to this problem include the design of an alternative control architecture (Kai et al., 2019) or a lower-dimensional attitude representation as done in Chaturvedi et al. (2009). The former authors design a continuous, time-invariant controller for attitude representations evolving on the two-sphere, denoted by $\mathbb{S}^2$. This attitude is referred to as reduced attitude (Chaturvedi et al., 2011), and shown to consitute a lower-dimension manifold of SO(3), where elements are invariant to rotations about a specified inertial axis. This makes it a suitable attitude representation for roll/pitch control, since the reduced attitude can be defined such that it is invariant to changes in the yaw angle.

Smooth geometric controllers on $\mathbb{S}^2$ have also been presented in Bullo et al. (1995) in the context of spin-axis stabilization of satellites. As continuous, time-invariant controllers, they suffer from vanishing proportional action close to additional undesired equilibra, which is a consequence of the topological obstruction to global stabilization that exist for any compact configuration manifold (Bhat and Bernstein, 2000). To overcome the resulting performance limitations (Chaturvedi et al., 2009) and to achieve global attitude stabilization, hybrid controllers for attitude tracking problems have appeared in Mayhew and Teel (2011) for quaternions and have recently been presented for $\mathbb{S}^n$ in Casau et al. (2019), with application to general rigid bodies and multirotor UAVs. The discussed controllers steer the attitude along the shortest possible path on the sphere, as opposed to controllers based on Euler angles. By using hybrid methods based on synergistic potential functions (Mayhew and Teel, 2013), robust and global exponential stability can be guaranteed. To the best of our knowledge, despite their desirable transient behaviour and stability properties, these methods have not been targeted at fixed-wing UAVs. The main contribution of this paper is to provide a suitable adaption for this type of aircraft. The aforementioned references control a body-fixed axis relative to an inertial frame, which is not directly applicable in a bank-to-turn maneuver. Instead, the direction of gravity relative to a body-fixed frame

⋆ This research was supported by the Research Council of Norway through the Centres of Excellence funding scheme, grant no. 223254 - NTNU AMOS, and no. 261791 AutoFly.

can be used, considering coupled dynamics in roll/pitch and a controller design that fits well into conventional autopilot architectures. Assuming bounded aerodynamic quantities which enter as exogeneous signals, we provide stability proofs to show global exponential tracking on $\mathbb{S}^2$ for the closed-loop system. This extends our work in (Coates et al., 2020).

2. PROBLEM FORMULATION

2.1 Notation

We represent the full attitude of the UAV by elements of the special orthogonal group of order three which defined as

$$\mathrm{SO}(3) = \{R \in \mathbb{R}^{3\times 3} : R^\top R = I, \det(R) = 1\}. \quad (1)$$

The matrix $R \in \mathrm{SO}(3)$ is referred to as a rotation matrix, and its columns describe axes of the body-fixed frame relative to an inertial reference frame. The two-sphere is embedded in $\mathbb{R}^3$ and defined by the set

$$\mathbb{S}^2 = \{x \in \mathbb{R}^3 : \|x\| = 1\}, \quad (2)$$

where $\|x\| = \sqrt{x^\top x}$ is the Euclidean norm of a vector x and $x^\top$ denotes the transpose. We let $\mathbb{R}_{\geq 0}$ and $\mathbb{N}$ denote the set of non-negative real and natural numbers, respectively, with $\mathbb{R}_{>0}$ as positive real numbers. The tangent space at a point $x \in \mathbb{S}^2$ is defined as the set of three-dimensional vectors that are orthogonal to x

$$\mathrm{T}_x\mathbb{S}^2 = \{y \in \mathbb{R}^3 : x \cdot y = 0\}. \quad (3)$$

Similarly, the normal space represents the space of all vectors parallel to x and can be defined as

$$N_x\mathbb{S}^2 = \{(z \in \mathbb{R}^3 : z \cdot y = 0,\ y \in \mathrm{T}_x\mathbb{S}^2\}. \quad (4)$$

Let the orthogonal projector $\Pi_x^\perp : \mathbb{S}^2 \mapsto \mathrm{T}_x\mathbb{S}^2$ and parallel projector $\Pi_x^\parallel : \mathbb{S}^2 \mapsto \mathrm{N}_x\mathbb{S}^2$ be defined as

$$\Pi_x^\perp = I - xx^\top,\ \ \Pi_x^\parallel = xx^\top, \quad (5)$$

such that the vector $y \in \mathbb{R}^3$ can be orthogonally decomposed to $y = \Pi_x^\perp y + \Pi_x^\parallel y$. Given two vectors $x, y \in \mathbb{R}^3$, the cross product can be represented as a matrix multiplication $x \times y = S(x)y$, where $S(x) = -S^\top(x)$ is the skew-symmetric matrix defined as

$$S(x) = \begin{bmatrix} 0 & -x_3 & x_2 \\ x_3 & 0 & -x_1 \\ -x_2 & x_1 & 0 \end{bmatrix}. \quad (6)$$

For vectors $x, y, z \in \mathbb{R}^3$, the following identities will be used:

$$x \cdot (y \times z) = y \cdot (z \times x) \quad (7)$$

$$\|x \times y\|^2 = \|x\|^2\|y\|^2 - (x^\top y)^2 \quad (8)$$

$$S^3(x) = -S(x) \quad (9)$$

$$x \times y = \|x\|\|y\| \sin(\theta) n, \quad (10)$$

where θ is the angle between x and y and n is the unit vector orthogonal to both vectors defined by the right-hand rule. For a more compact notation, we will only use time arguments when solutions or time-varying signals are considered.

2.2 Dynamic Model

The attitude dynamics of the UAV are given by

$$\dot{R} = RS(\omega) \quad (11)$$

$$J\dot{\omega} = S(J\omega)\omega + \tau, \quad (12)$$

where $\omega \in \mathbb{R}^3$ denotes the angular velocity in the body-fixed frame, $J = J^\top \in \mathbb{R}^{3\times 3}$ denotes the inertia matrix and $\tau \in \mathbb{R}^3$ is an external torque vector. Given aileron, elevator and rudder deflections δ_a, δ_e, $\delta_r \in \mathbb{R}$ we define the control input vector $u = [\delta_a, \delta_e, \delta_r]$ and model the torque in the control-affine form

$$\tau = f(\omega, v_r) + G(\omega, v_r)u, \quad (13)$$

where $v_r = [v_{r_1}\ v_{r_2}\ v_{r_3}]^\top \in \mathbb{R}^3$ denotes the (air-)relative velocity vector. The function $f(\omega, v_r)$ is the part of the attitude dynamics which is independent of u, sometimes referred to as drift term. The control effectiveness matrix $G(\omega, v_r) \in \mathbb{R}^{3\times 3}$ defines the aerodynamic coupling from the control surface deflections to the torque vector. This torque vector formulation is compatible with models in the standard literature, see e.g. Stevens et al. (2015), Beard and McLain (2012), which we briefly summarize now. Let $v_b \in \mathbb{R}^3$ be the linear velocity vector in the body-fixed frame and $w \in \mathbb{R}^3$ be the wind velocity vector in the inertial frame. Then the relative velocity vector is defined as $v_r = v_b - R^\top w$. It can be represented in terms of magnitude and spherical direction by

$$V_a = \|v_r\| = \sqrt{v_{r_1}^2 + v_{r_2}^2 + v_{r_3}^2} \quad (14)$$

$$\alpha = \mathrm{atan2}(v_{r_1}, v_{r_3}),\ \ \beta = \mathrm{atan2}(v_{r_2}, v_{r_1}) \quad (15)$$

with airspeed $V_a \in \mathbb{R}$, angle of attack $\alpha \in \mathbb{R}$ and sideslip angle $\beta \in \mathbb{R}$. They are used in the aerodynamic model in the general form

$$f(\omega, v_r) = \frac{1}{2}\rho V_a^2 S_{\text{wing}} \begin{bmatrix} bC_l(\alpha, \beta, \omega) \\ cC_m(\alpha, \beta, \omega) \\ bC_n(\alpha, \beta, \omega) \end{bmatrix} \quad (16)$$

$$G(\omega, v_r) = \frac{1}{2}\rho V_a^2 S_{\text{wing}} \begin{bmatrix} bC_{l_u}(\alpha, \beta, \omega) \\ cC_{m_u}(\alpha, \beta, \omega) \\ bC_{n_u}(\alpha, \beta, \omega) \end{bmatrix}, \quad (17)$$

where $\rho \in \mathbb{R}$ denotes the air density and $S_{\text{wing}}, b, c \in \mathbb{R}$ are the planform area, span and aerodynamic chord of the wings, respectively. Note that for a compact notation, we only include v_r in the function arguments, α and β follow from (15). The functions C_l, C_m, C_n are the aerodynamic coefficients for roll, pitch and yaw moment. The aerodynamic coefficients C_{l_u}, C_{m_u} and C_{n_u} map the control input to the resulting torque vector. For UAVs that are dependent on control surface deflections to deflect an airstream, a sufficiently large airspeed is needed to ensure controllability. This leads to the following assumption:

Assumption 1. Given a positive airspeed $V_a \geq \underline{V}_a \in \mathbb{R}_+$, the matrix $G(\omega, v_r)$ has full rank.

We also need an additional assumption to ensure that the torque vector is uniformly bounded:

Assumption 2. There exist constants $c_f, c_G > 0$ such that $\|f(\omega, v_r)\| \leq c_f$ and $\|G(\omega, v_r)\| \leq c_G$.

2.3 Reduced Attitude

We make use of the reduced-attitude vector $\Gamma \in \mathbb{S}^2$ as presented in Chaturvedi et al. (2011) and define it here as the representation of the vertical axis of the inertial frame $e_3 = [0\ 0\ 1]^\top$ expressed in the body-fixed frame

$$\Gamma = R^\top e_3. \quad (18)$$

The same reduced-attitude parametrization has been applied to stabilization of the inverted 3D pendulum (Chaturvedi et al., 2009). Note that the reduced-attitude vector is invariant to rotations about e_3 and therefore independent of yaw. In fact, given a roll angle $\phi \in [-\pi, \pi]$ and pitch angle $\theta \in [-\frac{\pi}{2}, \frac{\pi}{2}]$, the reduced-attitude vector can be parameterized as

$$\Gamma(\phi, \theta) = [-\sin\theta \quad \cos\theta \sin\phi \quad \cos\theta\cos\phi]^\top. \tag{19}$$

An orthogonal decomposition of the angular velocity vector $\omega = \omega^\perp + \omega^\parallel$ with respect to Γ can be obtained using (5) as

$$\omega^\perp = \Pi_\Gamma^\perp \omega \in \mathrm{T}_\Gamma\mathbb{S}^2, \;\; \omega^\parallel = \Pi_\Gamma^\parallel \omega \in \mathrm{N}_\Gamma\mathbb{S}^2. \tag{20}$$

The kinematics for Γ follows from (11) and (18) as

$$\dot{\Gamma} = \Gamma \times \omega = \Gamma \times \omega^\perp, \tag{21}$$

where the second equality results from $\omega = \omega^\perp + \omega^\parallel$ and $\Gamma \times \omega^\parallel = 0$. The derivative of (20) is given by

$$\dot{\omega}^\perp = \Pi_\Gamma^\perp \dot{\omega} + \omega^\perp \times \omega^\parallel \tag{22}$$

$$\dot{\omega}^\parallel = \Pi_\Gamma^\parallel \dot{\omega} + \omega^\parallel \times \omega^\perp. \tag{23}$$

2.4 Reference System

Consider a time-varying reference trajectory for the reduced attitude $\Gamma_d(t) \in \mathbb{S}^2$, satisfying

$$\dot{\Gamma}_d = \Gamma_d \times \omega_d \tag{24}$$

for some desired angular velocity $\omega_d(t) \in \mathrm{T}_{\Gamma_d}\mathbb{S}^2$. We assume that ω_d is twice continuously differentiable and that its derivative is uniformly bounded, i.e. there exist constants $c_{\omega_d}, c_{\dot{\omega}_d}$ such that

$$\omega_d(t) \in c_{\omega_d}\mathbb{B}, \qquad \dot{\omega}_d(t) \in c_{\dot{\omega}_d}\mathbb{B}, \tag{25}$$

where $\mathbb{B} = \{x \in \mathbb{R}^3 : \|x\| \leq 1\}$ is the closed unit ball in $\mathbb{R}^3$. The reasons for this assumption are twofold. First, the reference trajectory is smooth such that it may be used in feedforward-terms of the control law. And second, the differential inclusion of $\dot{\omega}_d(t)$ allows to formulate an autonomous closed-loop system such that hybrid invariance principles can be applied. We will also need the projection $\omega_d^\perp \triangleq \Pi_\Gamma^\perp \omega_d \in \mathrm{T}_\Gamma\mathbb{S}^2$, satisfying

$$\dot{\omega}_d^\perp = \Pi_\Gamma^\perp \dot{\omega}_d + \omega^\perp \times \Pi_\Gamma^\parallel \omega_d + \Pi_\Gamma^\parallel(\omega_d \times \omega^\perp). \tag{26}$$

An example of a reference filter that can be used to generate a reference trajectory $(\Gamma_d(t), \omega_d(t), \dot{\omega}_d(t))$ based on trajectories parametrized by Euler angles given in Appendix E.

2.5 Control Objective

It follows from (12), (13), (21) and (22) that only the part of the control input for which $J^{-1}G(\omega, v_r)u \in \mathrm{T}_\Gamma\mathbb{S}^2$ has an effect on the reduced attitude. The control objective is therefore to design a state feedback control law satisfying $J^{-1}G(\omega, v_r)u \in \mathrm{T}_\Gamma\mathbb{S}^2$ such that $\Gamma(t) \to \Gamma_d(t)$ and $\omega^\perp(t) \to \omega_d(t)$ as $t \to \infty$.

3. CONTROL ALGORITHM DESIGN

3.1 Hybrid Controller

We use the framework presented in Goebel et al. (2012) where a hybrid system can be defined as

$$(\dot{\xi}, \dot{q}) \in \mathcal{F}(\xi, q), \;\; \xi \in \mathcal{C} \tag{27}$$

$$(\xi^+, q^+) = \mathcal{G}(\xi, q), \;\; \xi \in \mathcal{D}, \tag{28}$$

with state $\xi \in \mathbb{R}^n$. When the state is inside the flow set $\mathcal{C} \subset \mathbb{R}^n$, its continuous motion is governed by the set-valued flow map $\mathcal{F} : \mathbb{R}^n \times Q \rightrightarrows \mathbb{R}^n \times Q$. Complementary, when the state is inside the jump set $\mathcal{D} \subset \mathbb{R}^n$ it evolves in the form of discrete jumps with its dynamics governed by the jump map $\mathcal{G} : \mathbb{R}^n \mapsto \mathbb{R}^n$. The variable $q \in Q$ is a discrete logic state. The hybrid time domain (t, i) consists of continuous time $t \in \mathbb{R}_{\geq 0}$ and jump time $i \in \mathbb{N}$. In the stability analysis of this section we will use the notation $V(t, i)$ instead of $V(\phi(t, i))$ where $\phi(t, i)$ denotes a solution to the system dynamics.

In the following we describe the design of a hybrid controller which employs proportional feedback based on a synergistic potential function as presented in Mayhew and Teel (2013), coordinated by a set of modes. The magnitude of the proportional feedback will depend on the gradient of the potential function in the active mode, which vanishes at the critical points of the potential function. The synergism property means that at all points other than the reference where this occurs, there is another mode in which the potential function has a significantly lower value. This solves the problem of vanishing proportional action at the the opposite direction of the reduced-attitude reference and renders the desired equilibrium globally asymptotically or exponentially stable, depending on the design of the sets $\mathcal{C}$ and $\mathcal{D}$.

3.2 Potential Function

The design of a synergistic potential function $\Psi : \mathbb{S}^2 \times \mathbb{S}^2 \times \mathbb{S}^2 \times Q \mapsto \mathbb{R}_{\geq 0}$ follows the approach presented in Lee (2016) to use two modes which gives the set $Q = \{0, 1\}$. The nominal mode $q = 0$ drives the reduced attitude in the direction of the nominal reference Γ_d. The expelling mode $q = 1$ will be designed such that the critical points of its potential function are at maximum distance to both the nominal reference and its antipodal pointi, i.e. they evolve on the unit circle on $\mathbb{S}^2$ orthogonal to Γ_d. Let the reference in the expelling mode be $s_d \in \mathbb{S}^2$ satisfying

$$\dot{s}_d = s_d \times \omega_d. \tag{29}$$

It follows from (24), (29) and the identity (7) that when s_d is initialized orthogonal to Γ_d, i.e. satisfies $s_d(0) \cdot \Gamma_d(0) = 0$, it holds that $s_d(t) \cdot \Gamma_d(t) = 0$ for all time.

In the following we let $\xi = (\Gamma, \omega^\perp, \Gamma_d, s_d, \omega_d) \in \Xi$ be the continuous state of the hybrid system which evolves in the space $\Xi \triangleq \mathbb{S}^2 \times \mathrm{T}_\Gamma\mathbb{S}^2 \times \mathbb{S}^2 \times \mathbb{S}^2 \times \mathrm{T}_{\Gamma_d}\mathbb{S}^2$. As in Mayhew and Teel (2013) we define the synergistic potential function as

$$\Psi_q(\Gamma, \Gamma_d, s_d) = \begin{cases} 1 - \Gamma \cdot \Gamma_d & \text{if } q = 0 \\ a + b(1 - \Gamma \cdot s_d) & \text{if } q = 1, \end{cases} \tag{30}$$

where the parameters $a, b \in \mathbb{R}_{>0}$ act as a bias and a scaling factor to the expelling potential which are designed such that Ψ_q is positive definite relative to Γ_d. The gradient of Ψ_q with respect to Γ is given by

$$\nabla_\Gamma \Psi_q(\Gamma, \Gamma_d, s_d) = \begin{cases} -\Gamma_d & \text{if } q = 0 \\ -b s_d & \text{if } q = 1. \end{cases} \tag{31}$$

Note that since $\mathbb{S}^2$ is a compact manifold and b is finite, $\|\nabla_\Gamma \Psi_q(\Gamma, \Gamma_d, s_d)\|$ is bounded.

3.3 Error States

The goal in either mode is to converge to the attitude with minimum potential along the shortest path on $\mathbb{S}^2$. This can be achieved by applying state feedback that is proportional to the gradient of the potential function with respect to Riemannian metric on $\mathbb{S}^2$. By (Bullo and Lewis, 2005, Lemma 11.6), the gradient vector field on $\mathbb{S}^2$ induced by Ψ_q is given by $\mathrm{d}\Psi_q(\Gamma) = S(\Gamma)^2\nabla_\Gamma\Psi_q$. It can be driven to zero by proportional feedback in the direction of the error vector

$$e_{\Gamma q} = -\Gamma \times \nabla_\Gamma \Psi_q(\Gamma, \Gamma_d, s_d) \in \mathrm{T}_\Gamma\mathbb{S}^2. \tag{32}$$

which can be interpreted as a rotation axis acting on Γ in the direction of $-\mathrm{d}\Psi_q(\Gamma)$ towards the reference. Let the angular velocity error $e_\omega \in \mathrm{T}_\Gamma\mathbb{S}^2$ be defined by

$$e_\omega = \omega^\perp - \Pi_\Gamma^\perp \omega_d, \tag{33}$$

which, using (22) and (26), can be shown to satisfy

$$\dot{e}_\omega = \Pi_\Gamma^\perp\Big(\dot{\omega} - \dot{\omega}_d + \omega^\perp \times (\omega^\parallel - \Pi_\Gamma^\parallel \omega_d)\Big) - \Pi_\Gamma^\parallel(\omega_d \times \omega^\perp). \tag{34}$$

Note that, even though $\omega^\perp$ and ω_d belong to different tangent bundles, the angular velocity error in (33) provides a valid comparison. This can be verified by showing that that the sufficiently smooth map $\Pi_\Gamma^\perp$ acts as a transport map following the definition given in Bullo and Murray (1999), which means that the equality

$$\nabla_r \Psi(\Gamma, \Gamma_d, s_d)^\top S(r) = -\nabla_\Gamma \Psi(\Gamma, \Gamma_d, s_d)^\top S(\Gamma)\Pi_\Gamma^\perp \tag{35}$$

needs to be satisfied for $r \in \{\Gamma_d, s_d\}$. Since this is the case, $\Pi_\Gamma^\perp$ is said to be compatible transport map to the potential function Ψ_q, which is essential in the stability proofs (Bullo and Lewis, 2005, Lemma 11.16).

3.4 Control Law

The control law is a combination of dynamic inversion, feedforward terms and PD-like feedback in terms of $e_{\Gamma q}$ and e_ω. It is defined as

$$u = G^{-1}(\omega, v_r) J\Big(-\Pi_\Gamma^\perp J^{-1}\big(f(\omega, v_r) + S(J\omega)\omega\big) + \kappa(\xi, q)\Big) \tag{36}$$

where $\kappa : \Xi \times Q \mapsto \mathrm{T}_\Gamma\mathbb{S}^2$ is defined as

$$\kappa(\xi, q) = -\omega^\perp \times (\omega^\parallel - \Pi_\Gamma^\parallel \omega_d) + \Pi_\Gamma^\parallel \dot{\omega}_d - k_p e_{\Gamma q} - \Pi_\Gamma^\perp K_d e_\omega, \tag{37}$$

with proportional gain $k_p \in \mathbb{R}_{>0}$ and positive definite gain matrix $K_d = {K_d}^\top \in \mathbb{R}^{3\times 3}$. The vector v_r is treated as a bounded exogeneous signal. Clearly, this control law only affects $\dot{\omega}^\perp \in \mathrm{T}_\Gamma\mathbb{S}^2$, as can be seen from (12) - (13). This leaves the possibility for an independent design of a control law $u^\parallel \in \mathrm{N}_\Gamma\mathbb{S}^2$ for other objectives such as turn coordination (Coates et al., 2020).

3.5 Jump Map

In the nominal mode, the error vector $e_{\Gamma q}$ drives the reduced attitude in the direction on the sphere that lies on the path of minimal distance between Γ and Γ_d, known as the minimal geodesic path (Bullo et al., 1995). To extend this path to the case where the expelling mode is active, s_d^+ is chosen as

$$s_d^+ \in g_{s_d}(\Gamma, \Gamma_d, s_d) \triangleq \begin{cases} \dfrac{\Gamma_d \times \Gamma}{\|\Gamma_d \times \Gamma\|} \times \Gamma_d & \text{if } \Gamma \neq \pm\Gamma_d \\ s_d & \text{otherwise} \end{cases} \tag{38}$$

which in the first case gives the point on $\mathbb{S}^2$ that lies on the geodesic path and satisfies the orthogonality constraint with respect to the nominal reference. The second case is included to ensure a well-defined solution.

3.6 Closed-loop System

We can now describe the closed-loop dynamics of the hybrid system. The continuous kinematics of Γ, Γ_d, s_d are given by (21), (24) and (29), respectively. The closed-loop dynamics for $\omega^\perp$ are given by (12), (13), (21), (22) and the control law (36). Both references are governed by the same kinematic equation as the reduced-attitude vector and the derivative of the angular velocity reference is included in $c_{\dot{\omega}_d}\mathbb{B}$ which allows for the formulation of an autonomous system (Mayhew et al., 2011). The resulting continuous motion of the closed-loop system is governed by

$$\begin{bmatrix} \dot{\Gamma} \\ \dot{\omega}^\perp \\ \dot{\Gamma}_d \\ \dot{s}_d \\ \dot{\omega}_d \\ \dot{q} \end{bmatrix} \in \mathcal{F}(\xi, q) \triangleq \begin{bmatrix} \Gamma \times \omega^\perp \\ \kappa(\xi, q) + \omega^\perp \times \omega^\parallel \\ \Gamma_d \times \omega_d \\ s_d \times \omega_d \\ c_{\dot{\omega}_d}\mathbb{B} \\ 0 \end{bmatrix}. \tag{39}$$

The discrete motion is independent of the control law and only has an effect on the mode and the expelling reference which results in jumps governed by

$$\begin{bmatrix} \Gamma^+ \\ \omega^{\perp +} \\ \Gamma_d^+ \\ s_d^+ \\ \omega_d^+ \\ q^+ \end{bmatrix} = \mathcal{G}(\xi, q) \triangleq \begin{bmatrix} \Gamma \\ \omega^\perp \\ \Gamma_d \\ g_{s_d}(\Gamma, \Gamma_d, s_d) \\ \omega_d \\ 1 - q \end{bmatrix}. \tag{40}$$

3.7 Hybrid Controller Sets

To coordinate the control laws, we use the difference between the potential of the current mode to the minimum potential, referred to as synergy gap by (Mayhew and Teel, 2013). It is defined as

$$\mu(\Gamma, q) = \Psi_q(\Gamma, \Gamma_d, s_d) - \min_{\nu \in Q} \Psi_\nu(\Gamma, \Gamma_d, s_d). \tag{41}$$

Let us further introduce the constant hysteresis parameter $\delta \in \mathbb{R}_{>0}$ to define the sets $\mathcal{C}, \mathcal{D} \subset \Xi \times Q$ as

$$\mathcal{C} = \{(\xi, q) : \mu(\Gamma, q) \leq \delta\}, \tag{42}$$

$$\mathcal{D} = \{(\xi, q) : \mu(\Gamma, q) \geq \delta\}. \tag{43}$$

The following proposition establishes conditions on the potential function such that it is synergistic and positive definite relative to Γ_d:

Proposition 1. Let the sets $\mathcal{C}, \mathcal{D}$ be given by (42) and (43), with synergy gap μ defined in (41). Then the potential function Ψ_q in (30) is a synergistic potential function with gap exceeding δ satisfying

$$0 < \delta < \min\{2 - a - b, a - 1, a + 2b - 1\}. \tag{44}$$

Proof. See Appendix A.

The closed-loop hybrid system is defined such that it satisfies the hybrid basic conditions (Goebel et al., 2012, Assumption 6.5) which makes it nominally robust to measurement noise. The next proposition provides a collection of these conditions.

Proposition 2. Consider the sets $\mathcal{C}$ in (42), $\mathcal{D}$ in (43) and the maps $\mathcal{F}$, $\mathcal{G}$ in (39),(40). Then, the following is satisfied:

(i) The sets $\mathcal{C}$ and $\mathcal{D}$ are closed.
(ii) The map $\mathcal{F}$ is outer semicontinuous and locally bounded relative to $\mathcal{C}$ and $\mathcal{F}(\xi, q)$ is convex for every $(\xi, q) \in \mathcal{C}$.
(iii) The map $\mathcal{G}$ is outer semicontinuous and locally bounded relative to D.

Proof. See Appendix B.

The stability results can be summarized in two propositions that need the following additional assumption:

Assumption 3. The parameters $a, b, \delta \in \mathbb{R}$ are such that Ψ_q in (30) satisfies (44) according to Proposition 1. Further, the time-varying reference trajectory $(\Gamma_d(t), s_d(t), \omega_d(t), \dot{\omega}_d(t))$ satisfies (24), (25) and (29).

Proposition 3. Let Assumption 1 and Assumption 3 hold. Consider the closed-loop hybrid system $\mathcal{H} = (\mathcal{C}, \mathcal{F}, \mathcal{D}, \mathcal{G})$ with $\mathcal{F}$, $\mathcal{G}$ defined in (39), (40) and the sets $\mathcal{C}$, $\mathcal{D}$ given by (42), (43). Then the set

$$\mathcal{A} = \{(\xi, q) \in \Xi \times Q : \Gamma = \Gamma_d,\ \omega^{\perp} = \omega_d\} \tag{45}$$

is globally asymptotically stable for $\mathcal{H}$.

Proof. See Appendix C.

It follows from (32) and (33) that inclusion in the set $\mathcal{A}$ implies $e_{\Gamma q} = 0$ and $e_\omega = 0$. An additional condition for inclusion in the jump set based on the angular velocity error can be shown to yield a stronger stability result. The next proposition summarizes the conditions for global exponential stability.

Proposition 4. Let Assumption 1 and Assumption 3 hold. Consider the closed-loop hybrid system $\mathcal{H} = (\mathcal{C}, \mathcal{F}, \mathcal{D}, \mathcal{G})$ with $\mathcal{F}$, $\mathcal{G}$ defined in in (39), (40) and the sets $\mathcal{C}$, $\mathcal{D} \subset \Xi \times Q$ given by

$$\mathcal{C} = \{(\xi, q) : \mu(\Gamma, q) \leq \delta \text{ or } \|e_\omega\| \geq B_{e_\omega}\}, \tag{46}$$
$$\mathcal{D} = \{(\xi, q) : \mu(\Gamma, q) \geq \delta \text{ and } \|e_\omega\| \leq B_{e_\omega}\} \tag{47}$$

where $B_{e_\omega} \in \mathbb{R}_{>0}$ is constant. Then the set

$$\mathcal{A} = \{(\xi, q) \in \Xi \times Q : \Gamma = \Gamma_d,\ \omega^{\perp} = \omega_d\} \tag{48}$$

is globally exponentially stable for $\mathcal{H}$.

Proof. See Appendix D.

Note in the proof to Proposition 4 that B_{e_ω} may be chosen arbitrarily large such that it does not necessarily impose practical limitations. Moreover, the sets $\mathcal{C}$ and $\mathcal{D}$ are closed and the maps $\mathcal{F}$ and $\mathcal{G}$ are not changed. The hybrid basic conditions are thus also satisfied for Proposition 4.

4. NUMERICAL EXAMPLE

We use the model of the Aerosonde UAV with the nonlinear aerodynamics as described in Beard and McLain (2012) and compare two controllers. First, a continuous controller that employs the nominal mode throughout the simulation and second, the presented hybrid controller that may switch to the expelling mode in addition. A stability analysis showing semiglobal exponential stability of the continuous controller is presented in Coates et al. (2020). The airspeed is treated as an exogeneous signal and controlled via a PI-Controller through the propeller throttle.

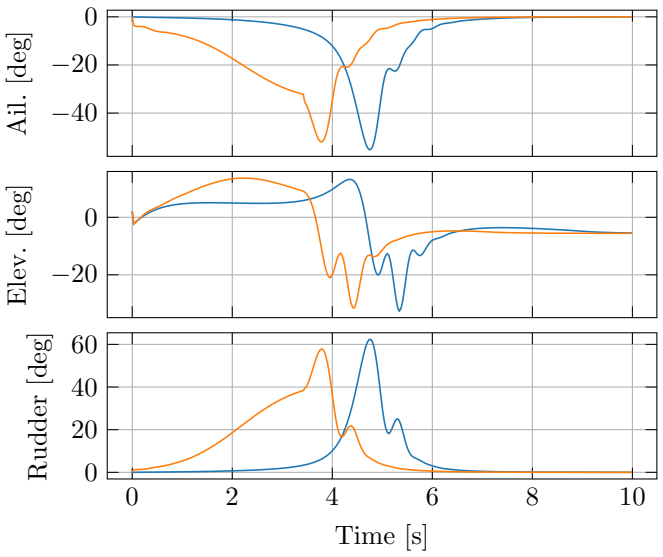

Fig. 1. Control surface deflections of aileron δ_a, elevator δ_e and rudder δ_r for the continuous controller (blue) and the hybrid controller (orange).

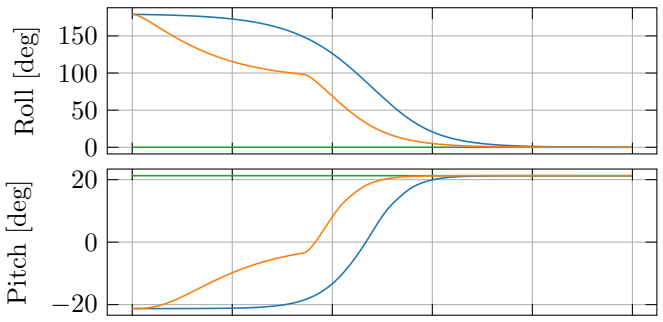

Fig. 2. Attitude response represented by the angles roll ϕ and pitch θ for the continuous controller (blue) and the hybrid controller (orange) including the reference (green).

The controller parameters are chosen as $k_p = 9.5$, $K_d = 8I_3$, $a = 1.25$, $b = 0.6$. We simulate the recovery from a large initial attitude disturbance and set the initial state such that $\Gamma(0) = -\exp(e_1\epsilon)\Gamma_d$ with $\epsilon = \pi/180$ and $e_1 = [1\ 0\ 0]^\top$. In terms of Euler angles, this corresponds a roll angle of -179 degrees and pitch angle of -21.26 degrees. The yaw angle is set to zero. The reference is parameterized according to (19) with zero roll angle and 21.26 degrees pitch angle, which is the trim condition for wings-level ascending flight at 35 meters per second airspeed. Note that the initial attitude is thus far from the given reference.

As shown in Fig. 2, the continuous controller remains close to the initial attitude up to 3 seconds whereas the hybrid controller reacts instantly and uses the expelling

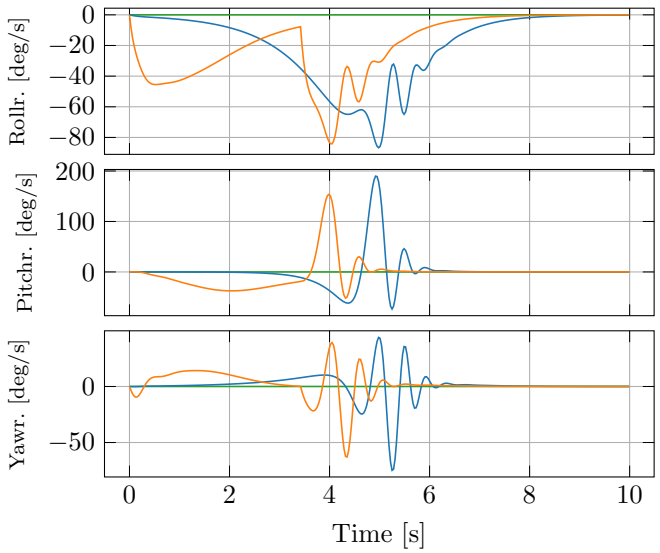

Fig. 3. Angular rate response represented by roll rate p, pitch rate q and yaw rate r for the continuous controller (blue) and the hybrid controller (orange) including the reference (green).

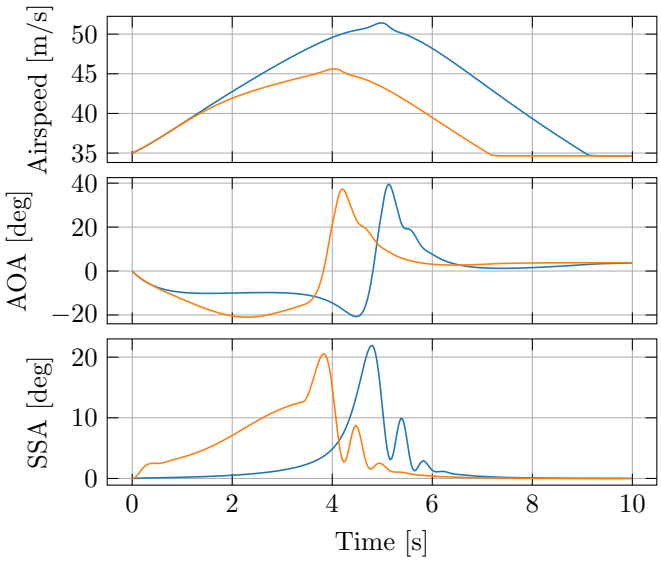

Fig. 4. Results of the relative velocity represented by airspeed V_a, angle of attack α (AOA) and sideslip angle β (SSA) for the continuous controller (blue) and the hybrid controller (orange).

potential with a larger gradient up to 3.5 seconds into the simulation before switching to the nominal potential (cf. Fig. 5). As a consequence, the hybrid controller recovers faster from the descend at a lower speed (cf. Fig. 4) and returns to ascending flight two seconds before the continuous controller, with similar actuator usage (cf. Fig. 1). A drawback of the hybrid controller however is the decceleration close to the expelling reference as shown in Fig. 3 and Fig. 5. This suggests using a dynamic extension in which the control action is given by a dynamic weighting of both configuration error vectors as done in Berkane et al. (2017) or Mayhew and Teel (2013). Future work will also address performance of the hybrid

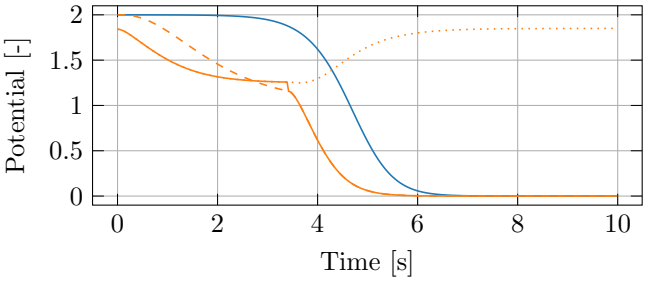

Fig. 5. Trajectories of the potential functions for the continuous controller (blue) and the hybrid controller (orange). The values for the nominal potential function Ψ_0 (dashed), the expelling potential function Ψ_1 (dotted), and the activated potential function Ψ_q (solid) are shown.

controller in the face of non-vanishing disturbances and model perturbations. Another aspect is the extension to the optimal use of the actuators while respecting saturation constraints, potentially in a model predictive control scheme.

Appendix A. SYNERGISTIC POTENTIAL FUNCTION

We first show that Ψ_q describes a synergistic potential function with synergy gap exceeding δ. This is to say that at every critical point other than the nominal reference the difference to the other potential function is larger than some specified δ. To this end, denote the set of critical points of Ψ_q for a fixed $q \in Q$ as

$$\mathrm{Crit}\Psi_q = \{(\Gamma, \Gamma_d, s_d) \in (\mathbb{S}^2)^3 : e_{\Gamma q} = 0\}. \tag{A.1}$$

From the definition of $e_{\Gamma q}$ it follows that at all critical points, the reduced attitude Γ is parallel to the gradient of the potential function $\nabla_\Gamma \Psi_q$. The set of all critical points follows as $\cup_{q\in Q}\mathrm{Crit}\,\Psi_\mathrm{q} = \{(\pm\Gamma_\mathrm{d}), (\pm\mathrm{s_d})\}$. For $\{\Psi_q\}_{q\in Q}$ to be centrally synergistic relative to Γ_d with gap exceeding δ, the condition $\cup_{q\in Q}\mathrm{Crit}\,\Psi_\mathrm{q}\backslash\{\Gamma_\mathrm{d}\} \subset \mathcal{D}$ needs to be satisfied. At $(\Gamma, q) = (-\Gamma_d, 0)$, the potential function evaluates to $\Psi_0(-\Gamma_d) = 2$ and $\Psi_1(-\Gamma_d) = a + b$, where we use the fact that $s_d \cdot \Gamma_d = 0$. To include that point in the jump set, the synergy gap needs to satisfy

$$\mu(-\Gamma_d, 0) = 2 - a - b > \delta > 0. \tag{A.2}$$

At the critical points of the expelling mode, the nominal potential evaluates to $\Psi_0(\pm s_d) = 1$ and for the expelling potential we have $\Psi_1(-s_d) = a + 2b$ and $\Psi_1(s_d) = a$. Therefore the synergy gap also has to satisfy

$$\mu(-s_d, 1) = a - 1 > \delta > 0 \tag{A.3}$$
$$\mu(+s_d, 1) = a + 2b - 1 > \delta > 0. \tag{A.4}$$

Then by (Mayhew and Teel, 2013, Proposition 1), the potential function Ψ_q is centrally synergistic relative to Γ_d with synergy gap exceeding δ given by (44).

Appendix B. PROOF OF PROPOSITION 2

To show that $\mathcal{C}$ and $\mathcal{D}$ are closed, note that Ψ_q is continuous for $q \in Q$ and that the minimum of two continuous functions is continuous. The synergy gap μ in (41) then is the difference of two continuous functions, which makes it continuous. Therefore the sets $\mathcal{C}$ and $\mathcal{D}$ are closed. The unit

ball $\mathbb{B}$ is compact and convex for any $(\xi, q) \in \mathcal{C}$ such that ω_d, $\dot{\omega}_d$ are bounded by assumption. All remaining components of $\mathcal{F}$ are continuous and single-valued functions on $\mathcal{C}$. Thus, the map $\mathcal{F}$ is convex and locally bounded relative to $\mathcal{C}$ and outer semicontinuity follows from (Goebel et al., 2012, Lemma 5.10), which shows (ii). Further, note that $\mathbb{S}^2$ is compact and hence $s_d^+ = g_{s_d}(\Gamma, \Gamma_d, s_d) \in \mathbb{S}^2$ is locally bounded relative to $\mathcal{D}$ and the graph of $g_{s_d} : \mathbb{S}^2 \times \mathbb{S}^2 \mapsto \mathbb{S}^2$ given by

$$\operatorname{gph} g_{s_d} = \{(\Gamma, \Gamma_d, s_d) \in \mathbb{S}^2 \times \mathbb{S}^2 \times \mathbb{S}^2 : s_d \in g_{s_d}(\Gamma, \Gamma_d, s_d)\} \tag{B.1}$$

is closed. Since $\mathcal{D}$ is closed, outer semiconituity of g_{s_d} relative to $\mathcal{D}$ follows from (Goebel et al., 2012, Lemma 5.10).

Appendix C. PROOF OF PROPOSITION 3

Given (30), (33) and (21) - (24), the closed-loop solution to Ψ_q can be shown to satisfy

$$\dot{\Psi}_q = e_{\Gamma q} \cdot e_\omega, \tag{C.1}$$

where (9) used. The time-derivative of the error vectors are given by

$$\dot{e}_{\Gamma q} = -S(\omega_d) e_{\Gamma q} + S(\nabla_\Gamma \Psi_q) S(\Gamma) e_\omega \tag{C.2}$$

$$\dot{e}_\omega = -k_p e_{\Gamma q} - \Pi_\Gamma^\perp K_d e_\omega - \Pi_\Gamma^\parallel (\omega_d \times e_\omega) \tag{C.3}$$

which can be found using (7), (22) and (26). To show asymptotic stability, let a Lyapunov function candidate be defined as

$$V = k_p \Psi_q + \frac{1}{2} {e_\omega}^\top e_\omega. \tag{C.4}$$

It follows from (C.1) and (C.3) that for $(\xi, q) \in \mathcal{C}$ along solutions of the closed-loop system, V satisfies

$$\dot{V}(t, i) = -{e_\omega}^\top \Pi_\Gamma^\perp K_d e_\omega \leq -\lambda_{\min}(K_d) \|e_\omega\|^2 \triangleq u_c(\xi). \tag{C.5}$$

It follows from K_d being positive definite that $u_c(\xi) \leq 0$ such that $V(t, i)$ is non-increasing along flows. In $\mathcal{D}$, the mode is switched to the lower potential which leads to the difference during jumps

$$V(t, i+1) - V(t, i) = -k_p \delta \triangleq u_d. \tag{C.6}$$

This shows that the growth of $V(t, i)$ along solutions to $\mathcal{H}$ is bounded by $u_c(\xi) \leq 0$ and $u_d < 0$. Note that by requiring the reference to be bounded, the dynamics of closed-loop system in (39) and (40) are autonomous and hybrid invariance principles can be applied. Then by (Goebel et al., 2012, Theorem 8.8) we have that for an arbitrary $c \in V(\Xi, Q)$ each precompact solution to $\mathcal{H}$ converges to the nonempty set that is the largest weakly invariant subset of

$$\Omega = V(c)^{-1} \cap \operatorname{cl}(u_c(0)^{-1}), \tag{C.7}$$

where $V(c)^{-1}$ denotes the preimage of the Lyapunov function candidate at c and $u_c(0)^{-1}$ denotes the preimage of u_c at 0 for which $\operatorname{cl}(u_c(0)^{-1})$ gives the closure. Then from (C.5) we see that $\operatorname{cl}(u_c(0)^{-1})$ leads to $e_\omega = 0$ which implies $\dot{e}_\omega = 0$. We substitute this into (C.3) to see that $e_{\Gamma q} = 0$ which gives $(\Gamma, q) \in \operatorname{Crit} \Psi$. Since all critical points except $(\Gamma_d, 0)$ are included in $\mathcal{D}$, it follows that $\mathcal{A}$ is the largest weakly invariant subset of Ω. Thus all precompact solutions of $\mathcal{H}$ converge to $\mathcal{A}$. Further note that $\mathcal{A}$ is compact and $\operatorname{cl}(\mathcal{C}) \cup \mathcal{D} = \Xi \times Q$ and therefore $\mathcal{G}(\mathcal{D}) \subset \operatorname{cl}(\mathcal{C}) \cup \mathcal{D}$. Since V is positive definite with respect to $\mathcal{A}$ it follows from (Goebel et al., 2012, Theorem 8.8) and (Goebel et al., 2012, Corollary 8.9 (iii)) that $\mathcal{A}$ is globally asymptotically stable.

Appendix D. PROOF OF PROPOSITION 4

This proof aim of the proof is to show global exponential stability as defined in (Teel et al., 2013). Along continuous flows and for bounds, Ψ_q and $e_{\Gamma q}$ are assumed for a fixed q, unless specified otherwise. We first show that the potential function is uniformly quadratic (Bullo and Murray, 1999). Since all critical points other than Γ_d are excluded from the flow set $\mathcal{C}$, there exists a constant γ such that the potential function can be bounded from above (see Lee (2015)) as

$$\Psi_q(\Gamma, \Gamma_d, s_d) \leq \frac{1}{2} \gamma \|e_{\Gamma q}\|^2. \tag{D.1}$$

To show a lower bound, we use scaling in each mode and define b_q as $b_0 = 1$ and $b_1 = b$. It then follows from (31) and (32), using (8) that the potential function is uniformly bounded by

$$\frac{1}{2 b_q} \|e_{\Gamma q}\|^2 \leq \Psi_q(\Gamma, \Gamma_d, s_d) \leq \frac{1}{2} \gamma \|e_{\Gamma q}\|^2. \tag{D.2}$$

Using (C.4), let a Lyapunov function be

$$V_\epsilon = V + \epsilon {e_\omega}^\top e_{\Gamma q} \tag{D.3}$$

for some $\epsilon \in \mathbb{R}_{>0}$. From (D.2) and defining $z = [\|e_{\Gamma q}\| \ \|e_\omega\|]^\top$ we see that V_ϵ can be bounded by

$$\frac{1}{2} z^\top M_1 z \leq V_\epsilon \leq \frac{1}{2} z^\top M_2 z, \tag{D.4}$$

where the matrices $M_1, M_2 \in \mathbb{R}^{2 \times 2}$ are given by

$$M_1 = \begin{bmatrix} \frac{k_p}{b_q} & -\epsilon \\ -\epsilon & 1 \end{bmatrix}, \qquad M_2 = \begin{bmatrix} k_p \gamma & \epsilon \\ \epsilon & 1 \end{bmatrix}. \tag{D.5}$$

Next, we show that there exists a $\lambda > 0$ such that along solutions of the closed-loop dynamics, V_ϵ can be bounded by

$$V_\epsilon(t, i) \leq V_\epsilon(0, 0) \exp(-\lambda t). \tag{D.6}$$

During jumps, the difference in V_ϵ is given by

$$V_\epsilon(t, i+1) - V_\epsilon(t, i) = -k_p \delta + \epsilon {e_\omega}^\top (e_{\Gamma q^+} - e_{\Gamma q}), \tag{D.7}$$

which can be bounded using (10) and the triangle inequality such that

$$\begin{aligned} &V_\epsilon(t, i+1) - V_\epsilon(t, i) \\ &\quad \leq -k_p \delta + \epsilon \|e_\omega\| \|\Gamma \times (\Gamma_d - b s_d)\| && \text{(D.8)} \\ &\quad \leq -k_p \delta + \epsilon \|e_\omega\| (\|\Gamma_d\| + |b| \|s_d\|) && \text{(D.9)} \\ &\quad \leq -k_p \delta + \epsilon B_{e_\omega} (1 + |b|). && \text{(D.10)} \end{aligned}$$

The right side of the last inequality is non-positive for

$$\epsilon \leq \frac{k_p \delta}{B_{e_\omega}(1 + |b|)}, \tag{D.11}$$

which shows that V_ϵ is non-increasing during jumps. Next we show that there exists a positive definite matrix $M_3 \in \mathbb{R}^{2 \times 2}$ such that along flows, V_ϵ satisfies

$$\dot{V}_\epsilon(t, i) \leq -z^\top M_3 z. \tag{D.12}$$

The upper bound of $\dot{V}$ is given by (C.5) and it remains to find a bound for the time-derivative of the cross-term in (D.3). From (C.2), (C.3) we see that

$$\begin{aligned} \frac{d}{dt}({e_\omega}^\top e_{\Gamma q}) &= {e_\omega}^\top (S(\nabla_\Gamma \Psi_q) S(\Gamma)) e_\omega - k_p \|e_{\Gamma q}\|^2 \\ &\quad - {e_{\Gamma q}}^\top (K_d + S(\omega_d)) e_\omega && \text{(D.13)} \\ &\leq \|\nabla_\Gamma \Psi_q\| \|e_\omega\|^2 - k_p \|e_{\Gamma q}\|^2 \\ &\quad + (\lambda_{\max}(K_d) + B_{\omega_d}) \|e_{\Gamma q}\| \|e_\omega\|, && \text{(D.14)} \end{aligned}$$

where (10) is used. From (C.5) and (D.12) follows

$$M_3 = \begin{bmatrix} \epsilon k_p & -\frac{\epsilon}{2}(\lambda_{\max}(K_d) + B_{\omega_d}) \\ -\frac{\epsilon}{2}(\lambda_{\max}(K_d) + B_{\omega_d}) & \lambda_{\min}(K_d) - \epsilon\|\nabla_\Gamma \Psi_q\| \end{bmatrix}. \tag{D.15}$$

The matrices M_1, M_2, M_3 are positive definite for any ϵ satisfying

$$\epsilon < \min_{q\in Q}\left\{ \sqrt{\frac{k_p}{b_q}}, \frac{4\lambda_{\min}(K_d)}{4k_p\|\nabla_\Gamma \Psi_q\| + (\lambda_{\max}(K_d) + B_{\omega_d})^2} \right\}, \tag{D.16}$$

which shows that (D.6) is satisfied for all initial conditions with $\lambda = \lambda_{\min}(M_3)$. We can then apply (Teel et al., 2013, Theorem 1) to conclude global exponential convergence of V_ϵ. Then $V_\epsilon = 0$ if and only if $\Psi_q = 0$ and $e_\omega = 0$ and hence $\Gamma \to \Gamma_d$ and $\omega^\perp \to \omega_d$, which shows that $\mathcal{A}$ is globally exponentially stable.

Appendix E. REFERENCE FILTER

An expression for the reduced-attitude vector Γ in terms of the Euler angles roll and pitch is given by (19). Differentiating leads to

$$\dot\Gamma = \begin{bmatrix} -\cos(\theta)\dot\theta \\ -\sin(\theta)\sin(\phi)\dot\theta + \cos(\theta)\cos(\phi)\dot\phi \\ -\sin(\theta)\cos(\phi)\dot\theta - \cos(\theta)\sin(\phi)\dot\phi \end{bmatrix}. \tag{E.1}$$

For $\omega^\perp \in \mathrm{T}_\Gamma\mathbb{S}^2$ we can invert (21) using (19) and (E.1) to get

$$\omega^\perp = \dot\Gamma \times \Gamma = \begin{bmatrix} \cos^2(\theta)\dot\phi \\ \cos(\phi)\dot\theta + \sin(\theta)\cos(\theta)\sin(\phi)\dot\phi \\ -\sin(\phi)\dot\theta + \sin(\theta)\cos(\theta)\cos(\phi)\dot\phi \end{bmatrix}, \tag{E.2}$$

with derivative

$$\dot\omega^\perp = \ddot\Gamma \times \Gamma, \tag{E.3}$$

where $\ddot\Gamma = [\ddot\Gamma_1,\ \ddot\Gamma_2,\ \ddot\Gamma_3]^\top$ can been found by differentiating (E.1), with elements given by

$$\ddot\Gamma_1 = \sin(\theta)\dot\theta^2 - \cos(\theta)\ddot\theta \tag{E.4}$$

$$\ddot\Gamma_2 = -\cos(\theta)\sin(\phi)(\dot\theta^2 + \dot\phi^2) - 2\sin(\theta)\cos(\phi)\dot\theta\dot\phi - \sin(\theta)\sin(\phi)\ddot\theta + \cos(\theta)\cos(\phi)\ddot\phi \tag{E.5}$$

$$\ddot\Gamma_3 = -\cos(\theta)\cos(\phi)(\dot\theta^2 + \dot\phi^2) + 2\sin(\theta)\sin(\phi)\dot\theta\dot\phi - \sin(\theta)\cos(\phi)\ddot\theta - \cos(\theta)\sin(\phi)\ddot\phi. \tag{E.6}$$

Given twice continuously differentiable reference trajectories $\phi_d(t), \theta_d(t)$ and their first and second derivatives (e.g. using third order linear reference filters (Fossen, 2011)), the relations (19) and (E.1) - (E.6) can be used to generate continuous signals $\Gamma_d(t)$, $\omega_d(t)$, $\dot\omega_d(t)$, which are needed to implement the tracking controller (36).

REFERENCES

Beard, R.W. and McLain, T.W. (2012). *Small unmanned aircraft: Theory and practice*. Princeton University Press.

Berkane, S., Abdessameud, A., and Tayebi, A. (2017). Hybrid global exponential stabilization on SO(3). *Automatica*, 81, 279–285.

Bhat, S.P. and Bernstein, D.S. (2000). A topological obstruction to continuous global stabilization of rotational motion and the unwinding phenomenon. *System & Control Letters*, 39(1), 63–70.

Bullo, F., Murray, R., and Sarti, A. (1995). Control on the sphere and reduced attitude stabilization. *IFAC Proceedings Volumes*, 28(14), 495–501.

Bullo, F. and Lewis, A.D. (2005). *Geometric Control of Mechanical Systems*, volume 49 of *Texts in Applied Mathematics*. Springer-Verlag.

Bullo, F. and Murray, R.M. (1999). Tracking for fully actuated mechanical systems: a geometric framework. *Automatica*, 35(1), 17–34.

Casau, P., Mayhew, C.G., Sanfelice, R.G., and Silvestre, C. (2019). Robust global exponential stabilization on the n-dimensional sphere with applications to trajectory tracking for quadrotors. *Automatica*, 110, 108534.

Chaturvedi, N.A., Lee, T., Leok, M., and McClamroch, N.H. (2011). Nonlinear dynamics of the 3D pendulum. *Journal of Nonlinear Science*, 21(1), 3–32.

Chaturvedi, N.A., McClamroch, N.H., and Bernstein, D.S. (2009). Asymptotic smooth stabilization of the inverted 3D pendulum. *IEEE Transactions on Automatic Control*, 54(6), 1204–1215.

Coates, E.M., Reinhardt, D., and Fossen, T.I. (2020). Reduced-attitude control of fixed-wing unmanned aerial vehicles using geometric methods on the two-sphere. In *2020 IFAC 21st World Congress*.

Fossen, T.I. (2011). *Handbook of marine craft hydrodynamics and motion control*. John Wiley & Sons.

Goebel, R., Sanfelice, R.G., and Teel, A.R. (2012). *Hybrid Dynamical Systems: Modeling, Stability, and Robustness*. Princeton University Press.

Johansen, T.A., Zolich, A., Hansen, T., and Sorensen, A.J. (2014). Unmanned aerial vehicle as communication relay for autonomous underwater vehicle - Field tests. *2014 IEEE Globecom Workshops (GC Wkshps)*, 1469–1474.

Kai, J.M., Hamel, T., and Samson, C. (2019). A unified approach to fixed-wing aircraft path following guidance and control. *Automatica*, 108, 108491.

Lee, T. (2015). Global exponential attitude tracking controls on SO(3). *IEEE Transactions on Automatic Control*, 60(10), 2837–2842.

Lee, T. (2016). Optimal hybrid controls for global exponential tracking on the two-sphere. In *2016 IEEE 55th Conference on Decision and Control (CDC)*, 3331–3337.

Mayhew, C.G., Sanfelice, R.G., and Teel, A.R. (2011). Quaternion-based hybrid control for robust global attitude tracking. *IEEE Transactions on Automatic Control*, 56(11), 2555–2566.

Mayhew, C.G. and Teel, A.R. (2011). Synergistic potential functions for hybrid control of rigid-body attitude. *Proceedings of the 2011 American Control Conference*, (3), 875–880.

Mayhew, C.G. and Teel, A.R. (2013). Global stabilization of spherical orientation by synergistic hybrid feedback with application to reduced-attitude tracking for rigid bodies. *Automatica*, 49(7), 1945–1957.

Stevens, B.L., Lewis, F.L., and Johnson, E.N. (2015). *Aircraft control and simulation: dynamics, controls design, and autonomous systems*. John Wiley & Sons.

Teel, A.R., Forni, F., and Zaccarian, L. (2013). Lyapunov-based sufficient conditions for exponential stability in hybrid systems. *IEEE Transactions on Automatic Control*, 58(6), 1591–1596.